Biochimica et Biophysica Acta 1798 (2010) 77–81

Contents lists available at ScienceDirect

Biochimica et Biophysica Acta

journal homepage: www.elsevier.com/locate/bbamem

Probing excited states and activation energy for the integral membrane protein phospholamban by NMR CPMG relaxation dispersion experiments

Nathaniel J. Traaseth [a], Gianluigi Veglia [a,b,*]

[a] Department of Biochemistry, Molecular Biology, and Biophysics, University of Minnesota, Minneapolis, MN 55445, USA
[b] Department of Chemistry, University of Minnesota, Minneapolis, MN 55445, USA

ARTICLE INFO

Article history:
Received 30 April 2009
Received in revised form 9 September 2009
Accepted 15 September 2009
Available online 23 September 2009

Keywords:
Phospholamban
NMR
Protein Dynamics
Relaxation Dispersion
Membrane Protein
Ca^{2+}-ATPase
SERCA
Solution NMR

ABSTRACT

Phospholamban (PLN) is a dynamic single-pass membrane protein that inhibits the flow of Ca^{2+} ions into the sarcoplasmic reticulum (SR) of heart muscle by directly binding to and inhibiting the SR Ca^{2+}ATPase (SERCA). The PLN monomer is the functionally active form that exists in equilibrium between ordered (T state) and disordered (R state) states. While the T state has been fully characterized using a hybrid solution/solid-state NMR approach, the R state structure has not been fully portrayed. It has, however, been detected by both NMR and EPR experiments in detergent micelles and lipid bilayers. In this work, we quantitatively probed the μs to ms dynamics of the PLN excited states by observing the T state in DPC micelles using CPMG relaxation dispersion NMR spectroscopy under functional conditions for SERCA. The ^{15}N backbone and $^{13}C_{\delta 1}$ Ile-methyl dispersion curves were fit using a two-state equilibrium model, and indicate that residues within domain Ia (residues 1–16), the loop (17–22), and domain Ib (23–30) of PLN undergo μs-ms dynamics ($k_{ex} = 6100 \pm 800\ s^{-1}$ at 17 °C). We measured k_{ex} at additional temperatures, which allowed for a calculation of activation energy equal to ~5 kcal/mol. This energy barrier probably does not correspond to the detachment of the amphipathic domain Ia, but rather the energy needed to unwind domain Ib on the membrane surface, likely an important mechanism by which PLN converts between high and low affinity states for its binding partners.

1. Introduction

Regulation of heart muscle contractility is a dynamic event requiring *molecular* control over the concentration of intracellular calcium. This process is primarily carried out by the ryanodine receptors, which release Ca^{2+} from the sarcoplasmic reticulum (SR), and Ca^{2+}-ATPase (SERCA), which pumps Ca^{2+} into the SR. SERCA is inhibited by an integral membrane protein phospholamban (PLN) in cardiac muscle [1]. Phosphorylation at Ser16 and/or Thr17 relieves inhibition, allowing for full viability of SERCA [2]. It has been shown that phosphorylated Ser16 PLN (pS16-PLN) causes a partial order-to-disorder transition resulting in an alteration of all four of the PLN dynamic domains: Ia (residues 1–16), loop (residues 17–22), Ib (residues 23–30), and II (residues 31–52) [3].

In the absence of SERCA, PLN exists in equilibrium between a dynamically ordered T state (Fig. 1, PDB *2KB7* [4]) and a dynamically disordered R state [5,6]. The T state is the most populated in both lipid bilayers and detergent micelles [7,8], having a population of 84% measured by EPR in DOPC/DOPE lipid bilayers [9]. While the T and R states are both able to bind SERCA [10], the R state likely has a higher affinity for the enzyme [11,12], as well as being necessary for recognition of its other binding partners, e.g., protein kinase A (PKA), Ca^{2+}/calmodulin-dependent kinase II (CAMKII), and A-kinase anchoring protein (AKAP) [13]. Understanding the dynamics for this T to R state equilibrium is necessary to rationalizing how these states play a role in SERCA regulation and thus Ca^{2+} concentrations within the cell.

NMR spin relaxation measurements give insight into local and global dynamics of proteins over a wide range of timescales (ps to s) under *native-like* conditions [14–18]. An important dynamic timescale that has been correlated with catalytic activity is μs to ms motion [19–24]. To probe this dynamics, the use of Carr–Purcell–Meiboom–Gill (CPMG) and spin-locking relaxation dispersion experiments ($T_{1\rho}$) are valuable [25–28]. In our previous work, we quantitatively characterized the dynamics of PLN on the ps to ns timescale and qualitatively showed PLN to exhibit slow dynamics [3,6]. In this study, we illustrate the kinetic and thermodynamic parameters for the PLN excited states by quantifying slow μs to ms dynamics using backbone ^{15}N and Ile-methyl group $^{13}C_{\delta 1}$ CPMG relaxation dispersion measurements.

2. Materials and methods

2.1. Protein production

A fully functional monomeric mutant of PLN (C36A, C41F, C46A, AFA-PLN) was expressed [U-^{15}N] and [$^{13}C_{\delta 1}$-Ile] using $^{15}NH_4Cl$ and 2-

Abbreviations: Phospholamban, PLN; sarco(endo)plasmic reticulum Ca-ATPase, SERCA; Carr–Purcell–Meiboom–Gill, CPMG

* Corresponding author. 321 Church St SE, Minneapolis, MN 55455, USA. Tel.: +1 612 625 0758.
E-mail address: vegli001@umn.edu (G. Veglia).

0005-2736/$ – see front matter © 2009 Elsevier B.V. All rights reserved.
doi:10.1016/j.bbamem.2009.09.009

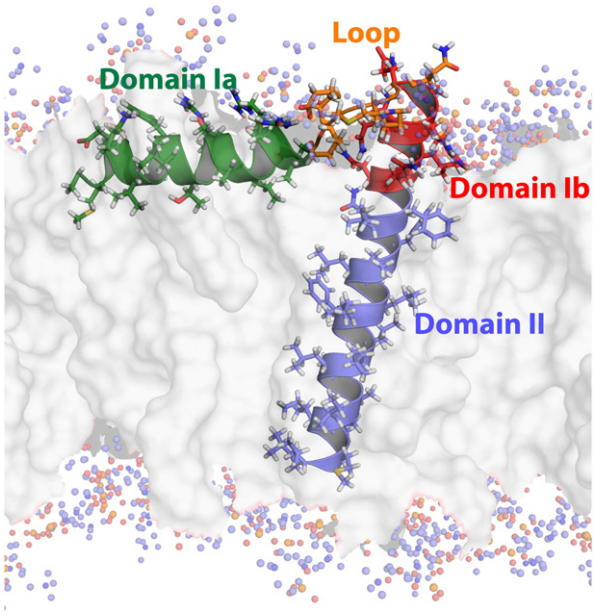

Fig. 1. Structure of the T state of monomeric AFA-PLN in a DOPC lipid bilayer derived from the hybrid solution and solid-state NMR method (*PDB 2KB7*) [4]. The four dynamic domains of AFA-PLN are denoted on the structure.

ketobutyric acid-4-^{13}C,3,3-d_2 (Isotec-Sigma/Aldrich), and purified as previously described [29,30]. After HPLC purification, the protein was lyophilized with the subsequent powder stored at −20 °C until sample preparation.

2.2. Sample preparation

AFA-PLN samples were dissolved to a concentration of 1 mM in 300 mM DPC, 120 mM NaCl, 20 mM sodium phosphate (pH 6.0), and 0.01% NaN_3 as previously used by our laboratory in several papers [3,30,31]. These samples were stable for several weeks over the temperature range used in these studies.

2.3. NMR spectroscopy

Spin relaxation experiments were performed using two AFA-PLN samples: 1) [U-^{15}N], [$^{13}C_{\delta1}$-Ile] and 2) [U-^{15}N]. Single quantum ^{15}N CPMG experiments with temperature compensation were carried out at $B_0 = 14.1$ and 18.7 T using relaxation compensated HSQC [32] and TROSY pulse sequences [33,34] with constant time delays of 20 and 40 ms, respectively. The 20 ms time was needed at 12 °C for the [U-^{15}N] sample to increase signal to noise. The time spacing between the 180° pulse centers is equal to $2\tau_{cp}$, which is expressed as a frequency (ν_{CPMG}) equal to $1/(4\tau_{cp})$. For the first sample, 2D datasets were acquired for $\nu_{CPMG} = 50(\times2)$, 100, 150, 200, 250, 300, 350, 400 (×2), 450, 500, 600, 700, 800, 900, 1000 (×2) Hz at $B_0 = 14.1$ and 18.7 T (at 17 °C). For the second sample, spectra were acquired in duplicate for $\nu_{CPMG} = 50$, 100, 150, 200, 300, 400, 500, 600, 700, 800, 900, and 1000 Hz at $B_0 = 14.1$ T, and in duplicate for $\nu_{CPMG} = 50$, 100, 200, 300, 400, 500, 600, 800, and 1000 Hz at $B_0 = 18.7$ T (at 17 °C). In order to assess the backbone exchange kinetics as a function of temperature, we acquired CPMG dispersion data at 12, 17, and 22 °C using a constant time delay of 20 ms in triplicate using $\nu_{CPMG} = 100$, 200, 300, 500, 700, and 1000 Hz at both $B_0 = 14.1$ and 18.7 T (see Supporting Information Fig. 1).

The ^{13}C multiple quantum relaxation experiments [35] were all performed at $B_0 = 14.1$ T with a constant time delay of 40 ms using ν_{CPMG} values at the following temperatures: 5 °C [50(×2), 100, 150, 700, 800, 900, 1000 (×2)], 10 °C, 20 °C, and 37 °C all with [50, 100 (×2), 150, 200, 250, 300 (×2), 350, 400, 450, 500, 600, 700, 800 (×2), 900, 1000 Hz]. Reference spectra were acquired with no constant time delay for each of the experiments.

Room temperature triple-axis gradient HCN Varian probes were used for all measurements, except one set of data using a [U-^{15}N] sample at $B_0 = 18.7$ T, in which a Varian cold-probe was used. Due to a slight detuning of the ^{15}N channel on the cold-probe at larger values of ν_{CPMG}, we applied a linear correction to those residues that showed dispersion (see Supporting Information Fig. 2). This correction was calculated from residues that did not show an exchange contribution to relaxation on the room temperature probes, and was relatively minor (~2 Hz difference in R_{2eff} for $\nu_{CPMG} = 50$ Hz and $\nu_{CPMG} = 1000$ Hz). R_{2eff} was calculated using the following relationship: $R_{2eff} = \frac{-ln\{I(\nu_{CPMG})}{I_0}\frac{1}{T}$, where $I(\nu_{CPMG})$ is the intensity for a given value of ν_{CPMG}, I_0 is the intensity of the reference spectrum, and T is the constant time delay. All errors reported in the figures are standard deviations from multiple experiments, or in cases where no duplicate or triplicate existed, the average of the standard deviation for points that were repeated.

A 100% methanol standard was used to calibrate the temperature on the spectrometers. All of the experiments were acquired with Varian spectrometers (VNMRS for $B_0 = 14.1$ T and INOVA for $B_0 = 18.7$ T), with the data processed in NMRPipe [36] and peak-picked in Sparky [37].

3. Results

Our previous data on the μs–ms dynamics on AFA-PLN were acquired at $B_0 = 18.7$ T and a temperature of 37 °C [3,6]. While these measurements qualitatively showed PLN to display slow dynamics, the ΔR_2 dispersions were rather small. In the new experiments, we first performed dispersion measurements at $B_0 = 14.1$ T and 37 °C, but found all residues to show dispersions < 2 Hz. As the temperature was

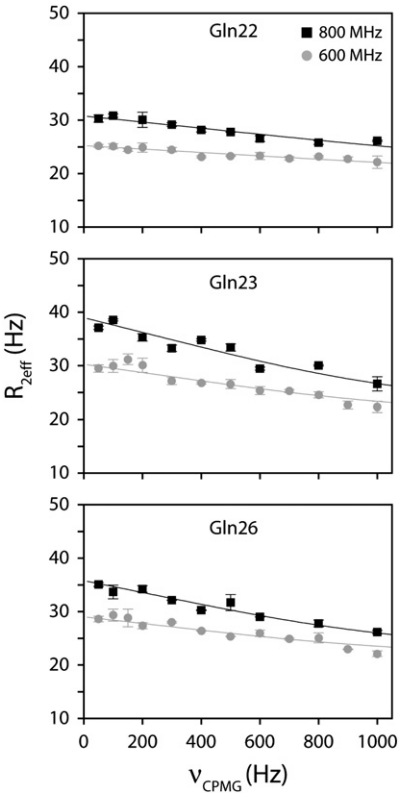

Fig. 2. ^{15}N CPMG dispersion curves at 600 (circles, 14.1 T) and 800 MHz (squares, 18.7 T) for selected residues of AFA-PLN at 17 °C. Best fits to Eq. (1) are plotted with the data. The error bars indicate the standard deviation from duplicate experiments at each value of ν_{CPMG}.

Table 1
Results from a global k_{ex} fit from ^{15}N single quantum dispersion curves using the fast chemical exchange equation (Eq. (1)).

k_{ex} (s^{-1})		
12 °C	17 °C	22 °C
6000 ± 600	6100 ± 800	8100 ± 700

The errors bars reflect an 85% confidence interval.

decreased to 22 °C and below, the dispersions became substantial for a number of residues. Interestingly, as the temperature was decreased from 37 °C, Thr17 and Ala24 became significantly broadened, which alone indicates a relaxation contribution from chemical exchange (R_{ex}), as anticipated by both NMR [3,6] and EPR data [5]. To assess k_{ex} as a function of temperature (12, 17, and 22 °C) we acquired ^{15}N dispersion curves at $B_0 = 14.1$ and 18.7 T. The data are shown in Fig. 2 and Supporting Information Fig. 1, where the error bars reflect the standard deviation between two (Fig. 2) or three identical experiments (Supporting Information Fig. 1) for each value of ν_{CPMG} collected in an interleaved manner.

A total of seven residues (Ser16, Thr17, Gln22, Gln23, Arg25, Gln26, and Asn27) display dispersion curves with $\Delta R_2 > 2$ Hz (i.e., dispersion), where $\Delta R_2 = R_{2eff}(\nu_{CPMG} = 50\ \text{Hz}) - R_{2eff}(\nu_{CPMG} = 1000\ \text{Hz})$. These residues are located within three domains of PLN (the loop and domains Ia and Ib). From the data shown in Fig. 2, ΔR_2 for $B_0 = 14.1$ and 18.7 T change by the expected quadratic scaling (~1.78) for fast exchange ($\Delta\omega^2$; see below). Therefore, all residues were fit to a two-site fast exchange model (Eq. (1)) to extract kinetic information from the dispersion curves [38].

$$R_{2eff}(\nu_{CPMG}) = R_2 + \frac{\varphi_{ex}}{k_{ex}}\left(1 - \frac{4\nu_{CPMG}}{k_{ex}}\tanh\left(\frac{k_{ex}}{4\nu_{CPMG}}\right)\right) \quad (1)$$

$\varphi_{ex} = p_A p_B \Delta\omega^2$, p_A and p_B are the populations of the two states, $\Delta\omega$ is the chemical shift difference between states A and B, k_{ex} is the exchange rate (sum of forward and reverse rate constants for the $A \Leftrightarrow B$ equilibrium), and R_2 is the intrinsic relaxation rate (assumed to be the same for states A and B). A least-squares fit to Eq. (1) was carried out in *Mathematica* to extract k_{ex}, R_2, and φ_{ex} for individual residues (at both magnetic fields) as well as a global fit [39]. The global fit was performed by simultaneously minimizing k_{ex} for all residues at both magnetic fields (Table 1). Importantly, the *global* k_{ex} values and the *average* values are in good agreement. The global k_{ex} values are 6000 ± 600 (12 °C), 6100 ± 800 s^{-1} (17 °C), and 8100 ± 700 for Ser16, Thr 17, Gln22, Gln23, Arg25, Gln26, and Asn27. The error bars reflect an 85% confidence interval.

As shown in Supporting Information Fig. 1, the HSQC-CPMG pulse sequence from Loria et al. [32] gave field-dependent R_2 values for all the residues, even those that did not experience chemical exchange (data not shown). In the absence of a correction factor, the data fitting

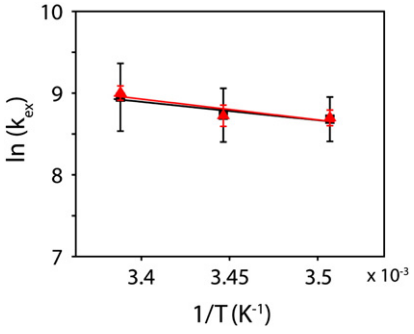

Fig. 3. Arrhenius plot for the ^{15}N CPMG dispersion data (red triangles—global k_{ex} fit; black squares—average k_{ex} values). Error bars reflect the 85% confidence interval from global fits and the standard deviation from averaging the residue-dependent k_{ex} values.

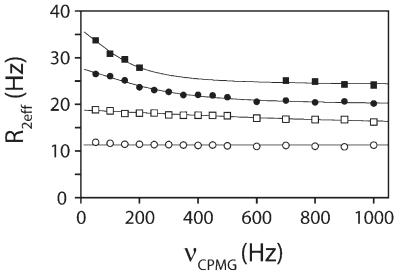

Fig. 4. Methyl group CPMG dispersion curves at $B_0 = 14.1$ T for Ile18 $^{13}C_{\delta1}$ for AFA-PLN at 5 °C (filled squares), 10 °C (filled circles), 20 °C (open squares), and 37 °C (open circles). Best fits to Eq. (1) assuming fast exchange are plotted with the data. The error bars are within the data points.

gave inconsistent values of k_{ex} relative to those determined using the TROSY CPMG sequence (no correction was needed for these experiments) [33,34]. For this reason, a correction factor was applied to R_2 for all residues experiencing chemical exchange in Eq. (1) (a global fit).

From the exchange rates reported in Table 1, an Arrhenius plot was constructed (Fig. 3) to determine the activation energy for the T state to an excited state. From the plot, we calculated an activation energy of ~5 kcal/mol.

In addition to the backbone ^{15}N CPMG dispersion curves, we also carried out dispersion analysis for Ile-methyl groups in AFA-PLN. Since the methyl groups are less sensitive to helical folding and more to electrostatic environment (hydrophobic packing, solvent structure, etc.), they are a better probe to test the solvent accessibility of PLN domains Ia and Ib. Within the Ile $^{13}C_{\delta1}$ spectra, the residues that gave dispersion were Ile12 and Ile18 (out of the 8 Ile methyl groups within PLN). Similar to the results for the backbone ^{15}N sites, Ile12 and Ile18 did not show significant dispersion at 37 °C at $B_0 = 14.1$ T. Upon decreasing the temperature, the methyl groups became quite sensitive to the dynamics, showing substantial dispersion (Fig. 4). Unfortunately, the Ile12 $^{13}C_{\delta1}$ resonance became substantially broadened at temperatures below 20 °C, leading to noisy dispersion data.

4. Discussion

The presence of the T and R states has been shown to be critical in the regulation of SERCA [10,12]. While the T state appears to be an inhibitory form of SERCA, the R state seems more important in the relief of SERCA regulation, as shown by Thomas and co-workers using an N-terminal lipid anchored PLN molecule (~100% T state) [10]. This knowledge encouraged the design of PLN mutants that might be able to lower the activation energy barrier to the R state, or simply increase the population of the R state, i.e., better mimic the R state [31]. This research is ongoing, and continues to be a promising path toward the design of therapeutic mutants that not only might overcome the effects of endogenous loss or gain-of-function PLN mutants, but also assist in the recovery of damaged heart muscle tissue.

Previously, our analysis of T_1, T_2, and heteronuclear NOE experiments for monomeric PLN showed the existence of two dynamically dissimilar domains within the single α-helix comprised of residues 22-52 [6]. The primary sequences of PLN agree well with this expected hydrophobic mismatch. Domain Ib is comprised of several hydrophilic and charged amino acids (Gln23, Ala24, Arg25, Gln26, Asn27, Leu28, Gln29, Asn30), while domain II is mainly comprised of hydrophobic amino acid residues (Leu, Ile, Val, and Phe). While the first structure reported by our laboratory in detergent micelles did not show the depth of insertion with respect to the membrane [7], our new structure exemplifies the dissimilarity of domains Ib and II in terms of dynamics and depth of membrane insertion (Fig. 1) [4,40]. The solvent exchange data also agree with this structure, as domain Ib

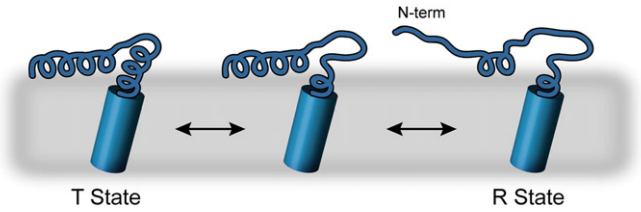

Fig. 5. Model of detaching/unfolding of monomeric PLN, which is consistent with CPMG dispersion data presented in this work as well as findings reported on the R state [42].

exchanges readily with H_2O, while domain II does not [7]. In fact, in perdeuterated growths of PLN [30], the majority of residues within domain II have attached deuterons to the amide nitrogen throughout the protein purification (3–4 days). Only upon unfolding of the protein and elevated temperature do these sites exchange with H_2O.

Domain Ib (residues 23–30) is well-known to be important in the regulation of SERCA [41]. Alanine-scanning mutagenesis indicates that most mutations in this region give rise to PLN mutants with gain-of-function, i.e., more inhibition [41]. In this work, we quantitatively assessed the chemical exchange of the T state of PLN, through the use of CPMG relaxation dispersion measurements. Our results indicate that several residues in domain Ib show dynamics in the μs to ms timescale. However, the observed exchange rates reported for PLN in Table 1 are not likely a simple exchange between T and R states, at least not for both amide backbone sites and side chain methyl groups. The reason is that in the methyl group spectrum of AFA-PLN, we detected both the T and R states for residues in domain Ia (i.e., slow exchange) [42]. Since we observed dispersion for Ile12 and Ile18 methyl groups at the $^{13}C_\delta$ position (Fig. 4), this means that the T state is in fast chemical exchange with another state. On the other hand, the backbone amide sites of the R state are not in slow exchange, which reflects the fact that the chemical shift differences ($\Delta\omega$) are smaller than for the methyl groups [11,12] Fig. 5 shows an unfolding model where we suggest an intermediate in the energy landscape toward the full R state. The first step depicts a partial unwinding of domains Ia and Ib (k_{ex} in fast chemical exchange) followed by a partial unwinding and detachment of domain Ia from the membrane (k_{ex} in slow chemical exchange [42]). This mechanism is similar to proposed models for the folding and unfolding of amphipathic antimicrobial peptides and proteins [43]. Therefore, assuming that domain Ib is similar in structure for the intermediate and final R state, the chemical exchange kinetics reported are reflective of the T to R state transition for backbone atoms, which would have an activation energy barrier of ~5 kcal/mol as measured by our CPMG experiments. Although this needs to be further investigated, domain Ib unwinding is supported by a model of PLN bound to SERCA (model by MacLennan and Toyoshima [44]) as well as the hypothesis that PLN needs to extend and potentially be pulled up from the membrane to interact with SERCA ([10]). The reported activation energy also is quite similar to those reported for amphipathic membrane peptides and proteins [43,45–50].

These new data further elucidate the dynamic picture of PLN, emphasizing the role of the loop and domains Ia and Ib in the partial unfolding process that may be needed to enable PLN to mold into the SERCA enzyme. The conformational dynamics of PLN is preserved in the presence of SERCA, where both T and R states have been detected by EPR [10]. Therefore, we propose that the inhibitory process occurs through a shift of the conformational equilibrium of T and R PLN states rather than through discrete (static) conformational states (free and bound).

Importantly, the conformational equilibrium of PLN between T and R states is *tunable* [31]. Ser16 phosphorylation of PLN, targeted mutations in the dynamic loop [31], and lipid membrane composition [51] have direct repercussions in SERCA affinity for calcium. In our recent paper [31], we used this information to design loss-of-function mutants of PLN to be tested in gene therapy, and proposed that new mutants must be promoted to the excited state (R state) for binding SERCA more effectively. In our previous work, however, we limited our functional manipulation and the rational mutagenesis to the dynamic loop of PLN. These new dynamics data implicate several residues in domains Ia and Ib that need to be incorporated to our existing knowledge database in order to design other PLN mutants that are more effective (better binder and loss-of-function) than the P21G mutant previously reported [31].

These studies stress the importance of dynamics in the functional characterization of the ground and excited states of small regulatory integral membrane proteins, enabling the progression of structural biophysics from *understanding* the biological phenomena to *controlling* the function.

Acknowledgments

We thank Martin Gustavsson and Lei Shi for stimulating discussion. This work was supported by NIH Grants (GM64742, HL80081, and GM072701) to G.V.

Appendix A. Supplementary data

Supplementary data associated with this article can be found, in the online version, at doi:10.1016/j.bbamem.2009.09.009.

References

[1] D.H. MacLennan, E.G. Kranias, Phospholamban: a crucial regulator of cardiac contractility, Nat. Rev. Mol. Cell Biol. 4 (2003) 566–577.
[2] A.D. Wegener, H.K. Simmerman, J.P. Lindemann, L.R. Jones, Phospholamban phosphorylation in intact ventricles. Phosphorylation of serine 16 and threonine 17 in response to beta-adrenergic stimulation, J. Biol. Chem. 264 (1989) 11468–11474.
[3] E.E. Metcalfe, N.J. Traaseth, G. Veglia, Serine 16 phosphorylation induces an order-to-disorder transition in monomeric phospholamban, Biochemistry 44 (2005) 4386–4396.
[4] N.J. Traaseth, L. Shi, R. Verardi, D. Mullen, G. Barany, G. Veglia, Determination of membrane protein structure and topology using a hybrid solution and solid-state NMR approach, Proc. Natl. Acad. Sci. 106 (2009) 10165–10170.
[5] C.B. Karim, T.L. Kirby, Z. Zhang, Y. Nesmelov, D.D. Thomas, Phospholamban structural dynamics in lipid bilayers probed by a spin label rigidly coupled to the peptide backbone, Proc. Natl. Acad. Sci. U. S. A. 101 (2004) 14437–14442 Electronic publication 2004 Sep 24.
[6] E.E. Metcalfe, J. Zamoon, D.D. Thomas, G. Veglia, $^{1}H/^{15}N$ heteronuclear NMR spectroscopy shows four dynamic domains for phospholamban reconstituted in dodecylphosphocholine micelles, Biophys. J. 87 (2004) 1–10.
[7] J. Zamoon, A. Mascioni, D.D. Thomas, G. Veglia, NMR solution structure and topological orientation of monomeric phospholamban in dodecylphosphocholine micelles, Biophys. J. 85 (2003) 2589–2598.
[8] N.J. Traaseth, J.J. Buffy, J. Zamoon, G. Veglia, Structural dynamics and topology of phospholamban in oriented lipid bilayers using multidimensional solid-state NMR, Biochemistry 45 (2006) 13827–13834.
[9] Y.E. Nesmelov, C.B. Karim, L. Song, P.G. Fajer, D.D. Thomas, Rotational dynamics of phospholamban determined by multifrequency electron paramagnetic resonance, Biophys. J. 93 (2007) 2805–2812.
[10] C.B. Karim, Z. Zhang, E.C. Howard, K.D. Torgersen, D.D. Thomas, Phosphorylation-dependent conformational switch in spin-labeled phospholamban bound to SERCA, J. Mol. Biol. 358 (2006) 1032–1040.
[11] N.J. Traaseth, D.D. Thomas, G. Veglia, Effects of Ser16 phosphorylation on the allosteric transitions of phospholamban/Ca(2+)-ATPase complex, J. Mol. Biol. 358 (2006) 1041–1050.
[12] J. Zamoon, F. Nitu, C. Karim, D.D. Thomas, G. Veglia, Mapping the interaction surface of a membrane protein: unveiling the conformational switch of phospholamban in calcium pump regulation, Proc. Natl. Acad. Sci. U.S.A. 102 (2005) 4747–4752 Electronic publication 2005 Mar 21.
[13] N.J. Traaseth, K.N. Ha, R. Verardi, L. Shi, J.J. Buffy, L.R. Masterson, G. Veglia, Structural and dynamic basis of phospholamban and sarcolipin inhibition of Ca(2+)-ATPase, Biochemistry 47 (2008) 3–13.
[14] A.G. Palmer III, C.D. Kroenke, J.P. Loria, Nuclear magnetic resonance methods for quantifying microsecond-to-millisecond motions in biological macromolecules, Methods Enzymol. 339 (2001) 204–238.
[15] L.E. Kay, Protein dynamics from NMR, Nat. Struct. Biol. 5 (Suppl) (1998) 513–517.
[16] D.A. Torchia, Solid state NMR studies of protein internal dynamics, Annu. Rev. Biophys. Bioeng. 13 (1984) 125–144.
[17] D.D. Boehr, H.J. Dyson, P.E. Wright, An NMR perspective on enzyme dynamics, Chem. Rev. 106 (2006) 3055–3079.

[18] J.W. Peng, G. Wagner, Investigation of protein motions via relaxation measurements, Methods Enzymol. 239 (1994) 563–596.
[19] F.A. Mulder, A. Mittermaier, B. Hon, F.W. Dahlquist, L.E. Kay, Studying excited states of proteins by NMR spectroscopy, Nat. Struct. Biol. 8 (2001) 932–935.
[20] H. Beach, R. Cole, M.L. Gill, J.P. Loria, Conservation of mus-ms enzyme motions in the apo- and substrate-mimicked state, J. Am. Chem. Soc. 127 (2005) 9167–9176.
[21] D.D. Boehr, D. McElheny, H.J. Dyson, P.E. Wright, The dynamic energy landscape of dihydrofolate reductase catalysis, Science 313 (2006) 1638–1642.
[22] D.Z. Kern, E.R., The role of dynamics in allosteric regulation, Curr. Opin. Struct. Biol. 13 (2003) 748–757.
[23] M.J. Grey, C. Wang, A.G. Palmer III, Disulfide bond isomerization in basic pancreatic trypsin inhibitor: multisite chemical exchange quantified by CPMG relaxation dispersion and chemical shift modeling, J. Am. Chem. Soc. 125 (2003) 14324–14335.
[24] E.Z. Eisenmesser, D.A. Bosco, M. Akke, D. Kern, Enzyme dynamics during catalysis, Science 295 (2002) 1520–1523.
[25] D.M. Korzhnev, L.E. Kay, Probing invisible, low-populated States of protein molecules by relaxation dispersion NMR spectroscopy: an application to protein folding, Acc. Chem. Res. 41 (2008) 442–451.
[26] A.G. Palmer III, F. Massi, Characterization of the dynamics of biomacromolecules using rotating-frame spin relaxation NMR spectroscopy, Chem. Rev. 106 (2006) 1700–1719.
[27] J.P. Loria, R.B. Berlow, E.D. Watt, Characterization of enzyme motions by solution NMR relaxation dispersion, Acc. Chem. Res. 41 (2008) 214–221.
[28] M. Akke, NMR methods for characterizing microsecond to millisecond dynamics in recognition and catalysis, Curr. Opin. Struct. Biol. 12 (2002) 642–647.
[29] B. Buck, J. Zamoon, T.L. Kirby, T.M. DeSilva, C. Karim, D. Thomas, G. Veglia, Overexpression, purification, and characterization of recombinant Ca-ATPase regulators for high-resolution solution and solid-state NMR studies, Protein Expr. Purif. 30 (2003) 253–261.
[30] N.J. Traaseth, R. Verardi, G. Veglia, Asymmetric methyl group labeling as a probe of membrane protein homo-oligomers by NMR spectroscopy, J. Am. Chem. Soc. 130 (2008) 2400–2401.
[31] K.N. Ha, N.J. Traaseth, R. Verardi, J. Zamoon, A. Cembran, C.B. Karim, D.D. Thomas, G. Veglia, Controlling the inhibition of the sarcoplasmic Ca2+-ATPase by tuning phospholamban structural dynamics, J. Biol. Chem. 282 (2007) 37205–37214.
[32] J.P. Loria, M. Rance, A.G.I. Palmer, A relaxation-compensated Carr–Purcell–Meiboom–Gill sequence for characterizing chemical exchange by NMR spectroscopy, J. Am. Chem. Soc. 121 (1999) 2331–2332.
[33] J.P. Loria, M. Rance, A.G. Palmer III, A TROSY CPMG sequence for characterizing chemical exchange in large proteins, J. Biomol. NMR 15 (1999) 151–155.
[34] P. Vallurupalli, D.F. Hansen, E. Stollar, E. Meirovitch, L.E. Kay, Measurement of bond vector orientations in invisible excited states of proteins, Proc. Natl. Acad. Sci. U.S.A. 104 (2007) 18473–18477.
[35] D.M. Korzhnev, K. Kloiber, V. Kanelis, V. Tugarinov, L.E. Kay, Probing slow dynamics in high molecular weight proteins by methyl-TROSY NMR spectroscopy: application to a 723-residue enzyme, J. Am. Chem. Soc. 126 (2004) 3964–3973.
[36] F. Delaglio, S. Grzesiek, G.W. Vuister, G. Zhu, J. Pfeifer, A. Bax, NMRPipe: a multidimensional spectral processing system based on UNIX pipes, J. Biomol. NMR 6 (1995) 277–293.
[37] T.D. Goddard and D.G. Kneller, SPARKY 3, University of California, San Francisco.
[38] Z. Luz, S. Meiboom, Nuclear magnetic resonance study of the protolysis of trimethylammonium ion in aqueous solution-order of the reaction with respect to solvent, J. Chem. Phys. 39 (1963) 366–370.
[39] E.L. Kovrigin, J.G. Kempf, M.J. Grey, J.P. Loria, Faithful estimation of dynamics parameters from CPMG relaxation dispersion measurements, J. Magn. Reson. 180 (2006) 93–104.
[40] L. Shi, N.J. Traaseth, R. Verardi, A. Cembran, J. Gao, G. Veglia, A refinement protocol to determine the structure, topology, and depth of insertion of membrane proteins using hybrid solution and solid-state restraints, J. Biomolec. NMR 44 (2009) 195–205.
[41] Y. Kimura, M. Asahi, K. Kurzydlowski, M. Tada, D.H. MacLennan, Phospholamban domain Ib mutations influence functional interactions with the Ca2+-ATPase isoform of cardiac sarcoplasmic reticulum, J. Biol. Chem. 273 (1998) 14238–14241.
[42] M. Gustavsson, N.J. Traaseth, E. Lockamy, D.D. Thomas and G. Veglia, Phosphorylation and pseudo-phosphorylation shift the phospholamban conformational equilibrium toward excited states, Submitted.
[43] P.F. Almeida, A. Pokorny, Mechanisms of antimicrobial, cytolytic, and cell-penetrating peptides: from kinetics to thermodynamics, Biochemistry 48 (2009) 8083–8093.
[44] C. Toyoshima, M. Asahi, Y. Sugita, R. Khanna, T. Tsuda, D.H. MacLennan, Modeling of the inhibitory interaction of phospholamban with the Ca2+ ATPase, Proc. Natl. Acad. Sci. U. S. A. 100 (2003) 467–472.
[45] J.F. Hunt, P. Rath, K.J. Rothschild, D.M. Engelman, Spontaneous, pH-dependent membrane insertion of a transbilayer alpha-helix, Biochemistry 36 (1997) 15177–15192.
[46] S.H. White, W.C. Wimley, Membrane protein folding and stability: physical principles, Annu. Rev. Biophys. Biomol. Struct. 28 (1999) 319–365.
[47] A.S. Ladokhin, S. Jayasinghe, S.H. White, How to measure and analyze tryptophan fluorescence in membranes properly, and why bother? Anal. Biochem. 285 (2000) 235–245.
[48] W. Meijberg, P.J. Booth, The activation energy for insertion of transmembrane alpha-helices is dependent on membrane composition, J. Mol. Biol. 319 (2002) 839–853.
[49] M. Fernandez-Vidal, S. Jayasinghe, A.S. Ladokhin, S.H. White, Folding amphipathic helices into membranes: amphiphilicity trumps hydrophobicity, J. Mol. Biol. 370 (2007) 459–470.
[50] D.I. Fernandez, J.D. Gehman, F. Separovic, Membrane interactions of antimicrobial peptides from Australian frogs, Biochim. Biophys. Acta 1788 (2009) 1630–1638.
[51] E. Hughes, J.C. Clayton, D.A. Middleton, Cytoplasmic residues of phospholamban interact with membrane surfaces in the presence of SERCA: a new role for phospholipids in the regulation of cardiac calcium cycling? Biochim. Biophys. Acta 1788 (2009) 559–566.